Simulation of a Micro-Scale Out-of-plane Compliant Mechanism

David Castro[1], Arpys Arevalo[*1], Ehab Rawashdeh[1], Nikolai Dechev[2] and Ian G. Foulds[1,3]
[1]King Abdullah University of Science and Technology,
Computer, Electrical and Mathematical Sciences and Engineering Division (CEMSE)
[2]University of Victoria, Department of Mechanical Engineering.
[3]The University of British Columbia, School of Engineering, Okanagan Campus
*Corresponding author: Thuwal 23955-6900, Kingdom of Saudi Arabia, arpys.arevalo@kaust.edu.sa

Abstract: In this work we present the simulation of a micro-scale large displacement compliant mechanism called the Tsang suspension. It consists of a flat micro-plate anchored down by two springs on either side, that can rotate out-of-plane and maintain its vertical assembly by a simple single-axis actuation. COMSOL was used to simulate these devices and extract the reaction forces of the springs throughout the process of an assembly. The effects of different design parameters were investigated to help designers understand the mechanical performance of such a structure.

Keywords: MEMS, SU-8, compliant mechanism.

1. Introduction

This paper investigates the effects of design parameter variation on the mechanical performance of the Tsang suspension [1,2]. Tsang suspensions are large displacement compliant mechanisms that can be assembled into out-of-plane configurations and provide a platform that can be used for various purposes. Tsang structures can be used in applications such as micro-mirrors [3], free-space optics [4-6] and RF systems [7]. Out-of-plane electro thermal actuators have been fabricated using the Tsang suspension, where an actuator design was connected to the springs instead of the plate [8]. Tsang suspensions have also been used in thermal isolation of sensors [9,10].

Similar out-of-plane structures, such as the so-called buckled cantilevers have been used to provide similar advantages for sensors and transducers [11-14]. However, the buckled cantilever needs a secondary structure such as an anchored stopper to maintain its 90˚ orientation to the substrate, while the Tsang suspensions create their own auto-locking mechanism due to the reaction force generated by the springs once the structure is assembled.

A Tsang suspension consists of a few elements, which are: anchor pads, two symmetrical spring beams, and a central platform (rectangular plate) as shown in Figure 1.

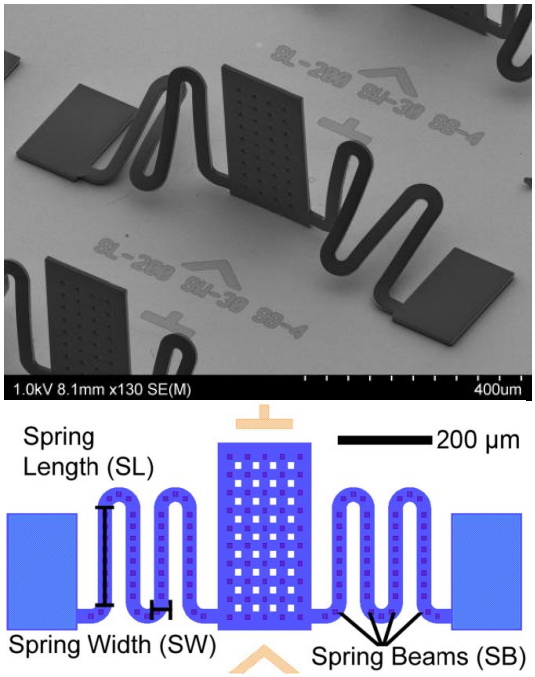

Figure 1. Top: SEM of an assembled SU-8 Tsang Suspension. Bottom: Illustration of Tsang suspension layout with Spring Length (SL) = 200 µm, Spring Width (SW) = 30 µm, Number of Spring Beams (SB) = 4.

Each spring beam is attached to the anchor pad at one end, and the unanchored central platform at the other end. The main advantage of this configuration is that it facilitates quick and easy assembly to achieve the final out-of-plane position. This is achieved by single-axis actuation via an external micromanipulator, by pushing with a probe tip at the bottom of the plate, which will produce an out-of-plane rotation into the final stable position.

Tsang suspensions are favorable for use, since they are easily fabricated using a single layer of micro-machined material. Further, they can be easily assembled using automated techniques, as described later in this paper. They have been fabricated out of different materials for various out-of-plane sensors and microsystems [3-8,11]. This includes micro-fabrication using SU-8 [11,13,14], poly (methyl methacrylate) (PMMA) [12], polysilicon [1,15], PMGI [16] and Polyimide [17-20].

To date, the design of previous Tsang suspensions has been ad-hoc, and no work has been presented to characterize and better understand how design parameters affect the mechanical performance of these structures. Therefore, the work described here was performed to characterize the design parameters through simulation to help in choosing the optimal parameters for the required application.

2. Design Parameters

The Tsang suspension is composed of symmetric springs, an unanchored platform, and the anchor pads (substrate), as shown in Figure 1. An in-plane force applied to the bottom edge of the central platform produces a complex deformation of the springs, which produces the desired out-of-plane motion of the platform. As a compliant mechanism, the geometry and dimensions of these springs will have a great impact on the structure's performance, and will therefore be the focus of this study.

The design parameters investigated in this work were: spring length (SL), spring width (SW), and the number of spring beams (SB), as shown in Figure 2. For short the notation {SL, SW, SB} will be used throughout the paper to refer to a specific design. For example, the notation {300, 20, 6} refers to a Tsang suspension with SL = 300 µm, SW = 20 µm, and SB = 6.

By varying SL, SW, and SB, the magnitudes of the reaction forces produced by the springs in the out-of-plane (z- direction) and in plane (y-direction) were studied. Also, the lateral displacement required to achieve a full out-of-plane rotation was studied.

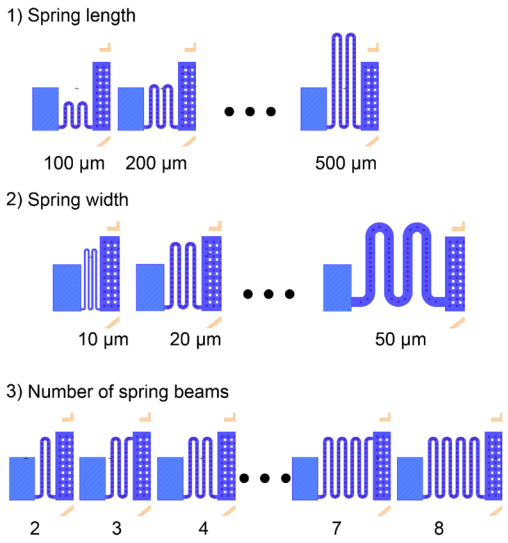

Figure 2. Representation of the parameters that will be varied.

In order to facilitate comparisons between various designs, a "standard design" Tsang suspension was established with the parameters SL = 200 µm, SW = 30 µm, and SB = 4 {200, 30, 4}. This was used as the basis point for the various parameter variations investigated. The standard design was chosen since experience with SU-8 has previously shown it as a reliable and stable design. Keeping two parameters fixed while changing the third, 10 different Tsang suspension designs were investigated, with variations of SL from 100 to 500 µm, SW from 20 to 50 µm and SB from 4 to 8, as shown in Table 1. Tsang suspensions with an odd number of spring beams have a fundamentally different behavior and therefore, were not studied in this work.

3. Use of COMSOL Multiphysics

One of the idiosyncrasies of Micro Electromechanical Systems (MEMS) is the fact that since device dimensions are small (typically < 1 mm), direct measurement of their mechanical properties can be challenging [21, 22]. Furthermore, this work deals with a large-displacement compliant mechanism with torsions, which can be quite complex to model analytically, and therefore a common solution is

to resort to nonlinear finite element modeling [23, 24].

The purpose of our simulations was to determine the stress within the Tsang structure, the reaction forces, and the displacement throughout its assembly process, which aren't readily accessible through experimentation or direct measurement alone. The simulation was conducted with Finite Element Analysis (FEA) using the COMSOL Multiphysics® software package. For simulation, the Tsang structures were first modeled using 3D computer aided design (CAD) software, and those designs were imported into COMSOL. The appropriate boundary conditions that represented the assembly process were applied, and the material properties were specified. The anchor pads were set such that the nodes in contact with the substrate were fixed (i.e. 0 displacement at those nodes in the x, y and z directions). The nodes representing the lower edge of the platform were constrained to allow for motion in the horizontal direction, but no motion in the vertical direction. This served to simulate the fact that the lower edge of the platform remains in contact with the substrate at all times. The actuation of the micromanipulator was simulated by applying a displacement boundary condition on the lower edge of the platform in the horizontal direction. The model was meshed with the automatic tetrahedron mesh tool, and analysis was done using the SPOOLES solver. Due to the large displacements involved with Tsang structures, the solver options for: (i) highly nonlinear and (ii) large deformation, were selected in the software. Figure 4 shows the simulation of an assembled Tsang suspension.

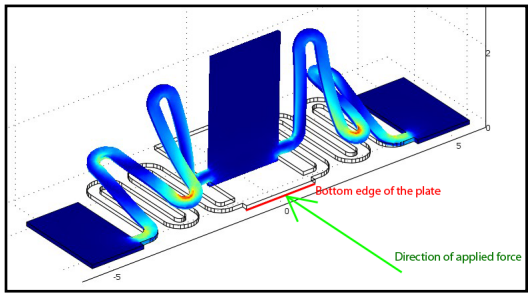

Figure 4.Tsang suspension assembly in COMSOL.

To validate the simulation's accuracy, matching structures were fabricated, and a Scanning Electron Microscope (SEM) was used to capture top-view images of the assembled structures. Figure 5 shows both an SEM image and a simulation screenshot of an assembled Tsang from the top. From this top-view image, the angle of selected spring beams was measured relative to a line drawn between the two anchor pads. This angle is denoted as θa and θb, for the simulation and SEM image, respectively. The comparison revealed an average difference between simulation θa and the experimental θb angle of 1.12% with a standard deviation of 0.75%. This provided confidence that the simulation adequately modeled the physical device.

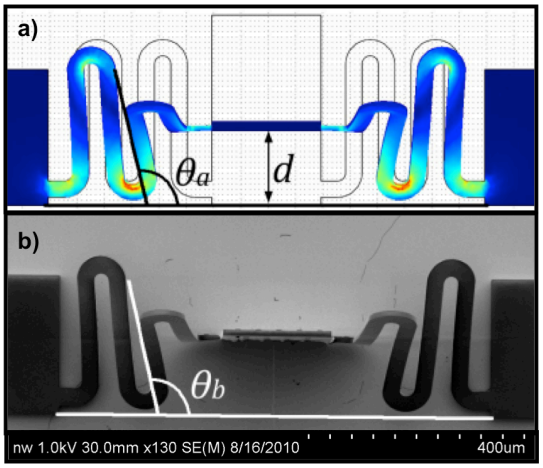

Figure 5. Top view of simulation and SEM image. An example comparison angle, "θa" and "θb", and displacement to vertical "d" are shown.

4. Simulations Results

The simulations were used to estimate the reaction forces of the Tsang structures, and further, to estimate the effect of parameter variation when designing the Tsang structures. During the assembly process, the direction of the spring reaction force changes as the rotation angle of the plate increases. This reaction force initially attempts to restore the plate to its original flat position (backwards). However, a critical "toggle point" (change-over point) is reached, where with further rotation, the reaction force begins to act downwards, thereby securing the plate in an out-of-plane orientation. The first step in the analysis of the Tsang structure was to determine the angle of rotation of the platform vs. the displacement of the lower edge of the

Table 1: Design outputs for all 10 of the studied variations.

Design	Lateral displacement required for assembly (µm)	Max RF_y (mN)	Max RF_z (mN)	Ratio of Max RF_z to Max RF_y	Minimum friction coefficient
{100,30,4}	105	1.3	1.39	1.06	0.32
{200,30,4}	148	0.69	0.74	1.08	0.31
{300,30,4}	190	0.39	0.42	1.07	0.32
{400,30,4}	240	0.25	0.26	1.07	0.30
{500,30,4}	285	0.17	0.18	1.06	0.32
{200,30,6}	162	0.39	0.41	1.04	0.28
{200,30,8}	175	0.24	0.24	1.01	0.35
{200,20,4}	130	0.54	0.55	1.02	0.34
{200,40,4}	160	0.81	0.91	1.12	0.26
{200,50,4}	170	0.89	1.02	1.15	0.30
Thickness variation*					
5 µm	142	0.97	0.11	1.12	0.26
15 µm	160	1.95	1.93	0.99	0.28
20 µm	175	3.76	3.47	0.92	0.35

** Represents a variation from the standard design {200, 30, 4}.*

platform. The results of one sample analysis for the design {200, 30, 4} are shown in Figure 6(a). Figure 6(b) shows the reaction forces acting on the lower edge of the plate for the same design, where Z denotes the vertical reaction force (RFz), and Y the horizontal reaction force (RFy). It can be seen that RFy increases to a maximum then decreases, while RFz increases throughout the assembly, reaching its maximum value when the plate has reached its final position. The decrease in RFy and increase in RFz is a desirable feature, as it shows the ability of the Tsang suspension to sustain its own assembly configuration. As reported previously [1], a measure of the structure's stability can be determined by the minimum coefficient of friction required to sustain assembly, given by the forces at the end of the rotation:

$$minimum\ friction\ coefficient \geq \frac{RF_{y,90^\circ}}{RF_{x,90^\circ}} \quad (1)$$

A similar parameter is the ratio between the maximum RFy and RFz reaction forces. The maximum RFy is the force required to assemble the device, while the maximum RFz maintains assembly. The ratio between these two forces is a measure of the conversion rate of the force applied during the assembly, into a desirable stabilizing force. Additional simulations that were not verified experimentally allowed exploring variations in the thickness of the springs. The results of these simulations are included and shown in Table 1.

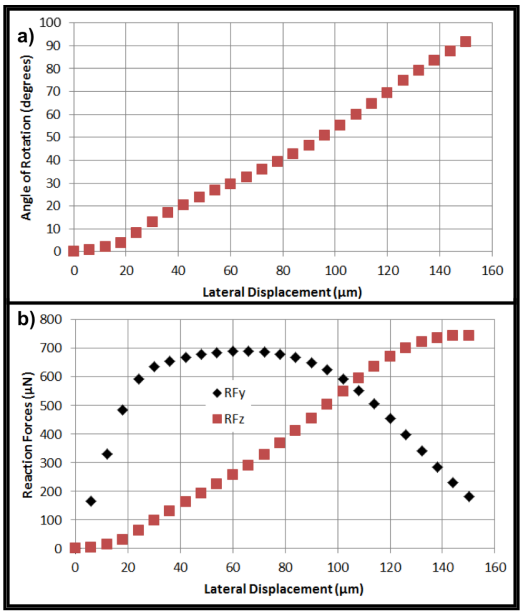

Figure 6. a) Angle of rotation versus lateral displacement of the Tsang suspension with SL = 200 µm, SW = 30 µm, SB = 4. b) Spring reaction force versus lateral displacement, with same design parameters.

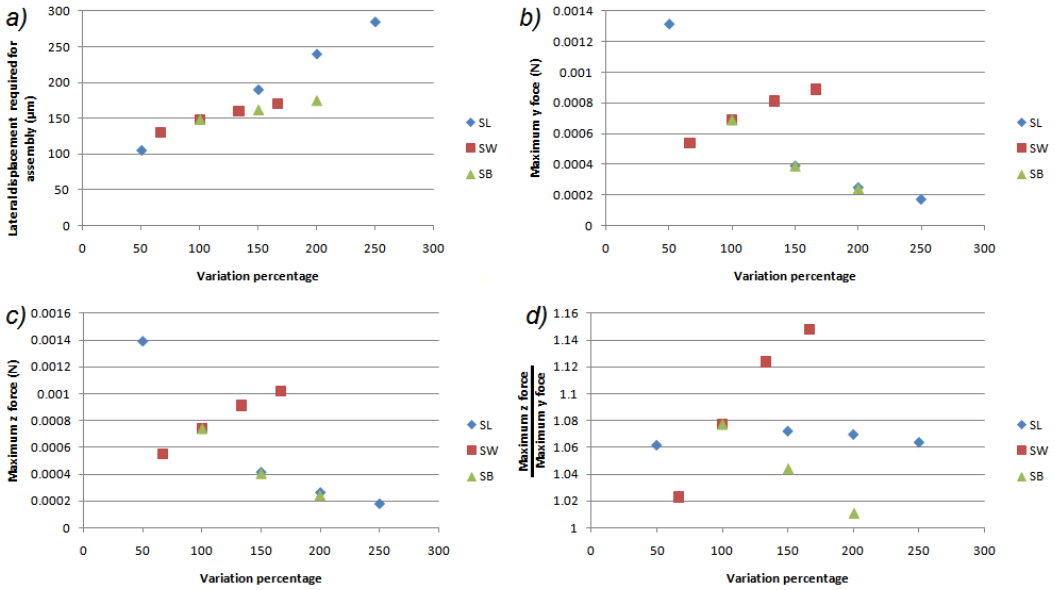

Figure 7. Graphs showing the effect of varying the different parameters as percentage variation of the standard design {200,30,4}.

In Figure 7, a graphical summary of the various design outcomes versus the change in parameters SL, SW and SB is provided. The design outcomes are: (a) Lateral displacement required for assembly, (b) Maximum y force, (c) Maximum z force, and (d) ratio of maximum z/y force. The horizontal axis of all plots is listed as a percentage, which is normalized with respect to the standard design {200, 30, 4}. For example, for variations in parameter SL, a value of 100% would represent SL = 200 since the SL of the standard design is 200. A value of 200 % would represent a design with SL = 400, and so forth. Each plot illustrates the effect of changing the three design parameters, with respect to a particular design outcome. For example, consider the effect of increasing the spring-beam length. Looking at the trends, it can be seen that increasing the spring-beam length will lead to an increase in the displacement required for assembly, as shown in Fig. 7(a). It will also lead to a decrease in the reaction forces in both z and y directions, as shown in Fig. 7(b) and (c), and has little effect on the Max RFz / Max RFy ratio, shown in Fig 7(d). As another example, increasing spring-beam width will result in an increase in all parameters.

5. Conclusions

The Tsang suspension and its design parameters were studied using COMSOL Multiphysics. By varying the spring length (SL), the spring width (SW) and the number of spring beams (SB), changes in the reaction forces and displacement required for assembly were determined. From our simulation results, we were able to generate graphs that can be used by designers unfamiliar with Tsang structures, to better understand the effect of changing a single parameter. The general trends observed were as follows. The in-plane reaction force of the springs (RFy) increases rapidly at the start of the assembly, reaches a maximum and gradually decreases. The out-of-plane reaction force (RFz) gradually increases throughout the assembly and reaches its maximum value when the platform approaches its vertical position. This change in the forces is desirable as it produces a self-sustaining vertical position on the platform structure, and keeps it in a stable position. An increase in any of the three parameters studied (spring length, spring width, and number of spring beams) will increase the structure's required lateral displacement, whereas reaction forces, RFy and RFz, increase if spring width increases, but decrease with the other parameters. Varying these parameters shows

only moderate effect on the structures stability as measured by the minimum required coefficient of friction. This work provides greater insight into their operation and provides designers with tools for designing their own implementation of the Tsang suspension.

6. References

1. S. H. Tsang, D. Sameoto, I. G. Foulds, R. W. Johnstone, and M. Parameswaran, "Automated assembly of hingeless 90 degrees out-of-plane microstructures," Journal of Micromechanics and Microengineering, vol. 17, no. 7, pp. 1314-1325. (2007)

2. Tsang, S. H., D. Sameoto, I. G, Foulds, A. M. Leung, and M. Parameswaran. "Wirebonder assembly of hingeless 90◦ out-of-plane microstructures." In Solid-State Sensors, Actuators, and Microsystems Workshop, Hilton Head Island, South Carolina, pp. 344-47. (2006)

3. S. Oak, G. F. Edmiston, G. Sivakumar, and T. Dallas, "Rotating Out-of-Plane Micromirror," Journal of Microelectromechanical Systems, vol.19, no.3, pp.632-639. (2010)

4. L. Y. Lin et al., "Micromachined integrated optics for free-space interconnections," Proc. IEEE Micro Electro Mechanical Systems (MEMS '95) pp 77–82. (1995)

5. M. C. Wu, "Micromachining for optical and optoelectronic systems," Proc. IEEE 85 1833–56. (1997)

6. L. Y. Lin et al., "Free-space micromachined optical switches with submillisecond switching time for large-scale optical crossconnects" IEEE Photon. Technol. Lett. 10 525–7. (1998)

7. D. J. Young et al., "Monolithic high-performance three- dimensional coil inductors for wireless communication applications" Technical Digest, Int. Electron Devices Meeting, pp 67–70. (1997)

8. S. H. Tsang et al., "Out-of-plane electrothermal actuators in silicon-on-insulator technology," Canadian Journal of Electrical and Computer Engineering, vol.31, no.2, pp.97-103. (2006)

9. S. H. Tsang et al., "Thin Film Transistor (TFT) Sensing Elements Fabricated in Surface Micromachined Polymermems for a Differential Calorimetric Flow Sensor," IEEE 22nd International Conference on Micro Electro Mechanical Systems, 2009. MEMS 2009. pp.583-586, 25-29 Jan. (2009)

10. S. H. Tsang et al., "Monolithically fabricated polymermems 3-axis thermal accelerometers designed for automated wirebonder assembly,"IEEE 21st International Conference on Micro Electro Mechanical Systems, 2008. MEMS 2008. pp.880-883, 13-17 Jan. (2008)

11. I. G. Foulds et al., "Polydimethylglutarimide (PMGI) as a sacrificial material for SU-8 surface-micromachining," Journal of Micromechanics and Microengineering, vol. 18, no. 7. (2008)

12. R. W. Johnstone et al., "Self-sacrificial surface micromachining using poly(methyl methacrylate)," Journal of Micromechanics and Microengineering, vol. 18, no. 11. (2008)

13. S. W. Lee et al., "Lithographic stress control for the self-assembly of polymer MEMS structures," Journal of Micromechanics and Microengineering, vol. 18, no. 8. (2008)

14. D. Sameoto et al., "Integrated Testing Of Polymer Mems Material Properties," in International Solid State Sensors and Actuators Workshop, Hilton Head Island, 2008, pp. 174-177. (2008)

15. S. Oak, "Testing and Characterization of 360° Rotating Out-of-Plane Micromirrors," Electrical Engineering, Texas Tech University, Lubbock. (2009)

16. I. G. Foulds et al., "Polydimethylglutarimide (PMGI) as a structural material for surface-micromachining," Journal of Micromechanics and Microengineering. vol. 18, no. 4, pp. 045026 (8pp). (2008)

17. L. Marnat, A. A. A. Carreno et al., "New Movable Plate for Efficient Millimeter Wave Vertical on-Chip Antenna," IEEE Transactions on Antennas and Propagation, vol. 61, pp. 1608-1615, April 2013. (2013)

18. A. Alfadhel, A. A. A. Carreno et al., "Three-Axis Magnetic Field Induction Sensor Realized on Buckled Cantilever Plate," Ieee Transactions on Magnetics, vol. 49, pp. 4144- 4147. (2013)

19. A. A. A. Carreno et al., "µHeater on a Buckled Cantilever Plate for Gas Sensor Applications", COMSOL Conference, Milan, Italy. (2012)

20. A. A. A. Carreno et al., "Optimized Cantilever-to-Anchor Configurations of Buckled Cantilever Plate Structures for Transducer Applications", COMSOL Conference, Milan, Italy. (2012)

21. T. Yi, and C. J. Kim, "Measurement of mechanical properties for MEMS materials", Measurement Science and Technology, 10(8), 706. (1999)

22. K. J. Hemker and W. N. Sharpe Jr, "Microscale characterization of mechanical properties", Annu. Rev. Mater. Res., 37, 93-126. (2007)

23. Howell, Larry L,"Compliant mechanisms", John Wiley & Sons, (2001)

24. Howell, Larry L. et al., "Handbook of compliant mechanisms". John Wiley & Sons. (2013)